STRUCTURE-PROPERTY RELATIONSHIPS IN COMPLEX FLUIDS: THE ROLE OF SIMULATIONS

DEBDAS DHABAL

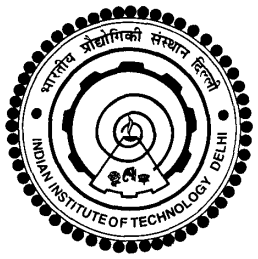

DEPARTMENT OF CHEMISTRY

INDIAN INSTITUTE OF TECHNOLOGY DELHI

MAY 2017

STRUCTURE-PROPERTY RELATIONSHIPS IN COMPLEX FLUIDS: THE ROLE OF SIMULATIONS

by

DEBDAS DHABAL

DEPARTMENT OF CHEMISTRY

Submitted

in fulfillment of the requirements of the degree of Doctor of Philosophy

to the

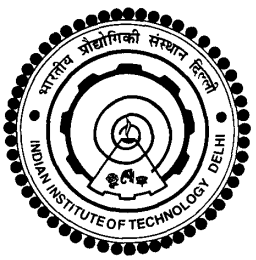

INDIAN INSTITUTE OF TECHNOLOGY DELHI

MAY 2017

To my Parents

and

our beloved Charu Ma'am
(Prof. Charusita Chakravarty)

Certificate

This is to certify that the thesis titled **"STRUCTURE-PROPERTY RELATIONSHIPS IN COMPLEX FLUIDS: THE ROLE OF SIMULATIONS"** is being submitted by **Mr. Debdas Dhabal** to the Department of Chemistry, Indian Institute of Technology Delhi, for the award of the degree of **Doctor of Philosophy**. This thesis is a record of bona-fide research work carried out by him under the supervision of (Late) Prof. Charusita Chakravarty from 21 July, 2011 to 29 March, 2016 and subsequently under our guidance. In our opinion, the thesis has reached the standards fulfilling the requirements of the regulations relating to the degree.

The results contained in this thesis have not been submitted to any other University or Institute for the award of any degree or diploma.

Prof. Ramakrishna Ramaswamy
Professor
School of Physical Sciences
Jawaharlal Nehru University
New Delhi-110 067, India

Dr. Hemant K. Kashyap
Assistant Professor
Department of Chemistry
Indian Institute of Technology Delhi
New Delhi-110 016, India

ACKNOWLEDGEMENTS

First and foremost, I would like to express my profound respect and heartfelt gratitude to Late Prof. Charusita Chakravarty. I am deeply grateful for her continuous guidance and supervision during my PhD work, without which it would have never been carried out successfully. Whatever knowledge I have in the field of computational chemistry and statistical mechanics is because of her consistent help, selfless support and constant encouragement. I feel blessed and honoured to be her student.

I am grateful to my current supervisor, Dr. Hemant K. Kashyap for his guidance and supervision over the past year, without which this thesis could not have been completed. His unconditional support and encouragement, as well as that of my co-supervisor Prof. Ram Ramaswamy, have helped to bring me to this stage. Thanks for being with me in my difficult times and for helping me to complete the thesis.

In addition to my supervisors, the work presented in this thesis would have been quite limited without support from many of my informed mentors. My special thanks to Prof. Valeria Molinero, Department of Chemistry, University of Utah, for taking time to guide me in writing manuscripts. Her commitment towards reading and commenting on manuscripts is highly appreciated. I would like to also thank Dr. Kjartan T. Wikfeldt for his genuine help and providing valuable inputs in experimental part of my work. I want to thank Dr. Lawrie Skinner for an outstanding research collaboration. It was my pleasure to visit Prof. Sanjoy Bandyopadhya's lab, at IIT Kharagpur, where I learned computational methods that have helped me a lot in my research work. Thanks to Mr. Prabir Khatua and Dr. Andrew H. Nguyen for helping me to learn the 2PT method used in this thesis.

I thank my Research Committee members Prof. A. K. Singh (Department of Chemistry), Dr. Pramit K. Chowdhury (Department of Chemistry), Prof. Bodh Raj Mehta (Department of Physics) for their timely evaluation, valuable suggestions and for asking interesting questions during my Comprehensive and Synopsis viva

which made me think beyond my work and helped me improve. I thank the faculty members of Chemistry Department and in particular Prof. A. Ramanan for helping me getting fellowship in the last few months.

I acknowledge University Grant Commission (UGC), India and IRD-IITD, India for financial support and CSC-IITD for high performance computing facilities.

The first 3 years of my lab were strongly coloured by a very close collaboration with my three "elders", Dr. Murari Singh and Dr. B. Shadrack Jabes and Dr. Divya Nayar, from whom I learned so many things related to computer simulations and related subjects. Thank you all for constantly listening me when I needed it and correcting my silly mistakes regarding research problems. This helped me to learn a lot. Special thanks to Divya Ma'am for fruitful discussions on some of my current research work. My appreciation also extends to my other lab colleagues; Madhulika for her genuine help; Hari Om (Sir) for useful discussions. I would like to thank my other lab-juniors; Aditya, Shobha, Supreet and Pratibha for their timely help. I also thank M.Sc project student, Sraddha Agarwal.

I take this opportunity to thank my friends whose support indirectly helped me in concentrating in my research work. A cordial thanks to Sandip, Sanjib, Tanmoy and Saurav for making me learning a coping mechanism to fight stress during my difficult times. Thanks for sharing many lifelong memories in IITD hostel days. I am also thankful to my childhood friends; Raju, Srimanta and Sudipta for being there for me in ups and downs of my life and always keeping me motivated to achieve something big.

Above ground, I am indebted to my family for their countless support which can not adequately be put in words. My deep love and affection to my parents (Baba and Ma); Shri Tapan Kumar Dhabal and Smt. Subhadra Dhabal for their constant support, sacrifice and blessing without which I could not have been able to finish this work. I thank my brothers; Achintya Kumar Dhabal (Choto dada) and Joydeb Dhabal (Boro dada) and sister in laws, whose sacrifice and love brings my strength and courage throughout my life. I take special pleasure in acknowledging my niece Rehanshi (Sonu) and my nephew Ritesh (Rishu) whose cute smile and sweet phone conversations always bring me inner strength and positivity about life.

Above all, thanks to almighty God for everything in my life.

Debdas Dhabal

Abstract

In this thesis, we examine the structural correlations, thermodynamics and dynamics of complex liquids using computer simulations. Water, a well-known tetrahedral liquid has been studied extensively. As a first step towards understanding the complexity of water, we use molecular dynamics (MD) and reverse Monte Carlo (RMC) simulation. In particular, we compute triplet correlation function which can probe the extent of tetrahedral network formation in liquids. We then estimate three body correlations in water from X-ray diffraction experiments and from molecular dynamics simulations using rigid-body (TIP4P/2005) as well as monatomic water (mW) models. MD results using rigid-body water model show good agreement with experiment. We estimate two-body and three-body contribution to the excess entropy for simple liquids as well as for a series of tetrahedral liquids (Si, Ge, SW_{16}) including water (mW), modeled with Stillinger-Weber potential. The two-phase thermodynamic (2PT) method, which is also a structure-based entropy estimation technique is used and compared with the thermodynamic estimator of excess entropy. The differences in crystallization and supercooling behavior of anomalous and simple liquids are discussed using the two-body and three-body contributions to the excess entropy and heat capacity. Structural, thermodynamic and dynamic anomalies are investigated in great detail for H_2O, Si and Ge. Comparison among the three liquids reveals that the structural order of liquids can affect the extent of anomalies in thermodynamic and dynamic properties. To understand the physical origin of anomalies, the relation between different liquid state anomalies has been examined. We also study room-temperature ionic liquids (RTILs) and high-temperature ionic melts (HTIMs) which are additional examples of important class of complex liquids. Triplet correlation functions and other structural measures are used to understand the differences in local morphology of RTILs and HTIMs. The studies presented in this thesis highlight the relationship between intermolecular interactions, atomic level structure and thermodynamic and dynamic properties of a large number of complex liquids.

सारांश

इस थीसिस में हमने जटिल तरल पदार्थ का संरचनात्मक सहसंबंध, उष्मिकी और गतिशीलता की जांच कंप्यूटर सिमुलेशन का उपयोग करते हुए किया है। जल , एक प्रसिद्ध टेट्राहेड्रल तरल का अध्ययन बड़े पैमाने पर किया गया है। जल की जटिलता को समझने के लिए पहले कदम के रूप में , हम आण्विक गतिशीलता (MD) और विपरीत मॉन्टे कार्लो (RMC) सिमुलेशन का प्रयोग किया है। विशेष रूप से, हम ट्रिप्लेट कोरिलेशन फंक्शन की गणना करते हैं जो जांच कर सकते हैं तरल पदार्थों में टेट्राहेड्रल नेटवर्क निर्माण की सीमा को! तथापि हम एक्स-रे विवर्तन और आण्विक गतिशीलता के प्रयोगों से TIP4P/2005 और साथ ही मोनो एटॉमिक वाटर (mW) में 3- बॉडी सहसंबंध को अनुमानित करते हैं। MD परिणाम रिजिड - बॉडी वाटर मॉडल के उपयोग से एक्सपेरिमेंट के साथ अच्छा समन्वय दिखाता है। हम 2-बॉडी और 3-बॉडी के लिए अतिरिक्त एन्ट्रॉपी में योगदान का अनुमान लगाते हैं, सरल तरल पदार्थ के साथ-साथ टेट्राहेड्रल तरल पदार्थों की एक श्रृंखला के लिए (Si, Ge, SW_{16}) एवम मोनो एटॉमिक वाटर (mW), जिसको स्टिलिंगर-वेबर क्षमता से मॉडल किया गया है। दो फेज ऊष्मप्रवैगिकीय (2PT) विधि, जो कि एक संरचना-आधारित एंट्रॉपी आकलन तकनीक भी है उपयोग किया जाता है और अतिरिक्त एन्ट्रापी के थर्मोडायनामिक अनुमानक के साथ तुलना की जाती है। क्रिस्टलीकरण और सुपरकुलिंग व्यवहार में अंतर विषम और सरल तरल पदार्थ के एन्ट्रापी और गर्मी क्षमता में 2-बॉडी एवम 3-बॉडी योगदानों के उपयोग पर चर्चा की जाती है। H_20, Si और Ge के लिए स्ट्रक्चरल, थर्मोडायनेमिक और गतिशील विसंगतियाँ महान विस्तार में जांच किया गया है । तीन तरल पदार्थों के बीच तुलना बताता है कि तरल पदार्थों का संरचनात्मक क्रम थर्मोडायनेमिक और गतिशील गुणों में विसंगतियों की सीमा को प्रभावित कर सकता है । विसंगतियों की भौतिक उत्पत्ति को समझने के लिए, विभिन्न तरल अवस्था की विसंगतियों के बीच संबंध की जांच की गई है। हम रूम-टेम्परेचर आयनिक तरल पदार्थ (RTILs) और उच्च तापमान वाले आयनिक मेल्ट्स (HTIMs) का भी अध्ययन करते हैं । ट्रिप्लेट कोरिलेशन फंक्शन और अन्य संरचनात्मक उपायों को समझने के लिए उपयोग किया जाता है RTILs और HTIMs के स्थानीय आकृति विज्ञान में अंतर का अध्ययन प्रस्तुत किया गया है । इस थीसिस में एक बड़ी संख्या में जटिल तरल पदार्थ के इंटरमॉलेकुलर इंटरैक्शन, एटॉमिक लेवल स्ट्रक्चर , थर्मोडिनामिक एवं गतिशीलता के बीच संबंध को उजागर करते हैं ।

Permissions

Permissions have been taken from the respective journals for the publications related to work presented in this thesis.

List of Publications Related to Work Presented in this Thesis as on Date of Submission of Thesis

1. B. Shadrack Jabes, Divya Nayar, **Debdas Dhabal** and Charusita Chakravarty, "Water and Other Tetrahedral Liquids: Order, Anomalies and Solvation", *J. Phys. Condens. Matter* **24**, 284116 (2012).

2. Murari Singh, **Debdas Dhabal**, A. Huy Nguyen, Valeria Molinero and Charusita Chakravarty, "Triplet Correlations Dominate the Transition from Simple to Tetrahedral Liquids", *Phys. Rev. Lett.* **112**, 147801 (2014).

3. **Debdas Dhabal**, Murari Singh, Kjartan T. Wikfeldt and Charusita Chakravarty, "Triplet Correlation Functions in Liquid Water", *J. Chem. Phys.* **141**, 174504 (2014).

4. **Debdas Dhabal**, A. Huy Nguyen, Murari Singh, Prabir Khatua, Valeria Molinero, Sanjoy Bandyopadhyay and Charusita Chakravarty, "Excess Entropy and Crystallization in Stillinger-Weber and Lennard-Jones Fluids", *J. Chem. Phys.* **143**, 164512 (2015).

5. **Debdas Dhabal**, Charusita Chakravarty, Valeria Molinero and Hemant K. Kashyap, "Comparison of Liquid-state Anomalies in Stillinger-Weber Model of Water, Silicon and Germanium", *J. Chem. Phys.*, **145**, 214502 (2016).

6. **Debdas Dhabal**, Kjartan T. Wikfeldt, Lawrie B. Skinner, Charusita Chakravarty and Hemant K. Kashyap, "Probing the Triplet Correlation Function in Liquid Water by Experiments and Molecular Simulations", *Phys. Chem. Chem. Phys.* **19**, 3265-3278 (2017).

7. **Debdas Dhabal**, Aditya Gupta and Hemant K. Kashyap, "Structural Investigation of Room-temperature Ionic Liquids and High-temperature Ionic Melts using Triplet Correlation Functions", *J. Chem. Phys.* **146**, 094503 (2017).

Contents

Certificate i

Acknowledgements iii

Abstract vii

Permissions ix

Table of Contents xi

List of Figures xvii

List of Tables xxxiii

1 Introduction 1

I General Background 3

1.1 Tetrahedral Liquids: A Simplest Category of Complex Liquids 8

1.2 Water: An Important Tetrahedral Liquid 9

1.2.1 Anomalies in Water 10

1.2.1.1 Thermodynamic Anomalies 11

1.2.1.2 Structural Anomaly 15

1.2.1.3 Transport Anomalies 16

1.2.2 Scenarios for Anomalies 17

1.2.3 Microscopic Structure of Liquid Water: Is it Really Tetrahedral ? 20

1.2.3.1 Recent Experimental and Simulation Studies on Structure of Water 22
1.3 *"Water-like"* Tetrahedral Liquids 27
1.3.1 Stillinger-Weber Liquids with Variable Tetrahedrality 27
1.4 Room-temperature Ionic Liquids 29
1.4.1 Phosphonium Ionic Liquids 32
1.5 Pair and Triplet Correlations and Structure - property Relationships in Liquids 33
1.5.1 Excess Entropy and Crystallization 39

II Systems and Computational Details 41

1.6 Partition Functions and Thermodynamic Potentials 41
1.7 Molecular Dynamics (MD) Simulations 43
1.8 Reverse Monte Carlo (RMC) Simulations 45
1.9 Systems Studied in this Thesis 49
1.9.1 Simple Liquids: Argon and Neon 49
1.9.2 Water 49
1.9.3 High-temperature Covalent Melts (HTCMs): Silicon and Germanium 51
1.9.4 Room-temperature Ionic Liquids (RTILs) 51
1.9.5 High-temperature Ionic Melts (HTIMs) 52
1.10 Estimation of Structural Order 53
1.10.1 Pair and Triplet Correlation Functions 53
1.10.2 Structure Factor 55
1.10.3 Angular Distribution Function 56
1.11 Entropy Estimation Methods 57
1.11.1 Widom Particle Insertion 57
1.11.2 Thermodynamic Integration (TI) 58
1.11.3 Multiparticle Correlation Expansion (MCE) Approximation . 62
1.11.4 Two-phase Thermodynamic(2PT) Method 63
1.12 Thermodynamic Response Functions 65

1.13 Transport Properties 66
1.14 Motivation and Organization of the Thesis 68

2 Triplet Correlation Functions Contain Information on Tetrahedrality of Liquid Water 73

2.1 Introduction 73
2.2 Molecular Dynamics Details 76
2.2.1 Rigid-body Water Models: SPC/E and TIP4P/2005 76
2.2.2 Monatomic Water (mW) Model 76
2.3 Reverse Monte Carlo Simulations 76
2.4 Results and Discussions 78
2.4.1 Total Structure Factors 78
2.4.2 Angular Distribution Functions 79
2.4.3 Tetrahedral Order Distributions 80
2.4.4 Equilateral Triplet Correlation Functions (ETCFs) and Kirkwood Superposition Approximations (KSA) 81
2.4.4.1 O-O-O Triplet, $g^{(3)}_{OOO}(r,r,r)$: 81
2.4.4.2 H-O-H Triplet, $g^{(3)}_{HOH}(r,r,r)$ 83
2.4.4.3 O-H-O Triplet, $g^{(3)}_{OHO}(r,r,r)$ 84
2.4.5 Isosceles Triplet Correlation Functions (ITCFs), $g^{(3)}_{OOO}(r,r,t)$. 85
2.5 Conclusions 87

3 Experimental Probe of Triplet Correlation Functions in Water: Comparison with Molecular Simulations 91

3.1 Introduction 91
3.2 Structure Factor and Triplet Correlation Function (TCF) 95
3.3 Numerical Evaluation of Structural Order 100
3.3.1 Structure Factor 100
3.3.2 Full Triplet Function, $\tilde{H}(q)$ 101
3.4 Molecular Dynamics Simulations 103
3.5 Experimental Details 106
3.6 Results and Discussions 107

3.6.1 O-O Structure Factor . . . 107
3.6.2 Triplet Function and Its Components . . . 107
3.6.3 Triplet Correlation Function . . . 114
3.6.4 Angular Distribution Function . . . 116
3.6.5 Tetrahedral Order Distribution . . . 117
3.7 Conclusions . . . 117

4 Excess Entropy and Crystallization in Simple and Anomalous Tetrahedral Liquids: Water, Silicon and Germanium 121
4.1 Introduction . . . 121
4.2 Molecular Dynamics Simulations . . . 126
4.2.1 Excess Entropy Estimation using Widom Insertion Method . . 127
4.2.2 Excess Entropy Estimation using TI Method . . . 128
4.2.3 Excess Entropy Estimation from 2PT Method . . . 128
4.2.4 Evaluation of Pair and Triplet Correlation Entropies . . . 130
4.3 Results and Discussions . . . 130
4.3.1 Response Function Behavior in Pair-dominated and Triplet-dominated Fluids . . . 130
4.3.2 Changes in Excess Entropy Associated with Supercooling and Comparison of Excess Entropy Obtained from Different Methods 133
4.3.3 Pair and Triplet Entropic Contribution to Heat Capacity . . . 135
4.3.4 Correlation Between S_{trip} and S_e . . . 137
4.3.5 Changes in Local Orientational Order prior to Crystallization 138
4.4 Conclusions . . . 140

5 Liquid-state Anomalies in Stillinger-Weber Model of Water, Silicon and Germanium 143
5.1 Introduction . . . 143
5.2 Molecular Dynamics Simulation . . . 146
5.2.1 MD Set1: Thermodynamics, Structural Quantities and Calculation of Diffusivity . . . 146
5.2.2 MD Set2: Viscosity and Conductivity Calculation . . . 149

5.3 Results and Discussions . . . 150
5.3.1 Water-like Anomalies in SW liquids . . . 150
5.3.1.1 Density Anomaly . . . 150
5.3.1.2 Entropy Anomaly . . . 152
5.3.1.3 Structural Anomaly . . . 154
5.3.1.4 Transport Anomalies . . . 155
5.3.1.5 Relation between Anomalies and Order-map . . . 157
5.3.2 Excess Entropy Scaling and Sequence of Anomalies . . . 158
5.3.3 Cascades of Anomalies . . . 162
5.3.4 Anomalies and Phase Diagram . . . 168
5.4 Conclusions . . . 171

6 Structural Investigation of Room-temperature Ionic Liquids and High-temperature Ionic Melts using Triplet Correlation Functions 175
6.1 Introduction . . . 175
6.2 Computational Details . . . 179
6.3 Results and Discussions . . . 182
6.3.1 Pair Correlation Functions (PCFs) . . . 182
6.3.2 Total and Partial Structure Functions . . . 184
6.3.3 Spatial Distribution Functions (SDFs) . . . 185
6.3.4 Triplet Correlation Functions (TCFs) . . . 186
6.3.4.1 Equilateral Triplet Correlation Functions (ETCFs) . 186
6.3.4.2 Isosceles Triplet Correlation Functions (ITCFs) . . . 192
6.4 Conclusions . . . 199

7 Summary and Future Perspectives 203

Bibliography 208

Biodata of the Candidate

List of Figures

1.1 One component phase-diagram of Lennard-Jones fluids in the pressure temperature ($P-T$) plane. A zoomed version of the solid-fluid coexistence and liquid-gas coexistence lines have been shown in the inset. The solid lines are the results from Ref. 6 and 7, while the the circles are from Barroso *et al.* [8]. The figure has been adapted from Ref. 8 with permission. 5

1.2 Representational view of pair correlation function of a simple liquids, showing the first, second and third coordination shells. 6

1.3 Approximate charge distribution of water molecule. Scale of positive and negative charge is given in the upper left corner. The figure is taken from Ref. 14. 10

1.4 Experimental density of water as a function of temperature at 1 atm pressure. Upon isobaric heating, there is an increase in density up to a point which is defined as temperature of maximum density, TMD (4 ^{o}C). The figure has been adopted from Ref. 21. 12

1.5 Schematic representation of water's best-known anomalies reported in the literature [10, 14, 17, 21, 26, 28]. Anomaly in (a) density (ρ), (b) excess entropy (S_e), (c) isobaric heat capacity (C_P), (d) thermal expansion coefficient (α_P), (e) isothermal compressibility (κ_T), (f) tetrahedral order parameter (q_{tet}), (g) diffusivity (D), (h) viscosity (η) and (i) thermal conductivity (κ) are depicted. Note that the simple liquid behavior is denoted using blue-coloured dashed line whereas anomalous behavior is designated using red-coloured line. 14

1.6 Defining structurally anomalous region: (a) Schematic representation of change in order parameters with change in density and corresponding structurally anomalous region. (b) The order map showing correlation between translational and tetrahedral order for SPC/E model of water. The figures (a) and (b) are adopted with permission from references 31 and 10 respectively. 15

1.7 Transport anomalies in liquid water, (a) experimental viscosity data of water as a function of pressure at different temperatures, (b) thermal conductivity as a function of temperature from experiment as well as from simulation. The figures (a) and (b) are adopted with permission from references 36 and 37 respectively. 17

1.8 Scenarios put forward to explain the origin of anomalies in water; (A) Stability limit conjecture, (B) liquid-liquid critical point scenario, (C) critical point free scenario and (D) singularity free hypothesis. The figure is adopted from Ref. 47. 19

1.9 (a) Experimental vapour-phase water dimer measured by Dyke *et al.* [48, 49]. Black dashed line is the symmetry axis of H-acceptor water molecule, red dashed line represents hydrogen bonding between the two water molecules. Oxygen-oxygen inter-molecular distance is depicted using blue line. (b) Local tetrahedral arrangements of water molecules as a consequence of hydrogen bonding interaction. Black dashed line represent H-bond between two water molecules. 21

1.10 Different partial pair correlation functions (PCFs) obtained from neutron diffraction and H-D substitution experiment performed by Narten and coworkers. Reprinted with permission from Ref. 72, data are originally taken from Ref. 71. 23

1.11 Tetrahedral ordering of water using X-ray Raman and X-ray emission spectroscopy (XRS and XES), (a) XRS spectra of liquid water at two different temperature and (b) SES spectra of liquid D_2O and H_2O at 280 K. Both the figures are adopted from Ref. 77 with permission. . . 25

1.12 Schematic representation of hydrogen-bonding pattern within the first coordination shell of water as interpreted by Wernet *et al.* [51] using XAS data. Two types of hydrogen atoms are shaded with different colors. H_2 with darker color represents that it is more electronegative than that of H_1 and has reduced capability to participate in further hydrogen bonding with other water molecules. The figure is adopted from Ref. 78. 26

1.13 Tetrahedrality-temperature ($\lambda - T$) phase diagram of the Stillinger-Weber liquids at zero pressure. Temperature is in reduced units with the depth of the pair potential serving as the unit of energy. The locus of points at which $S_2 = S_3$ is shown with open black squares and separates pair-dominated and triplet-dominated regimes. The locus of temperatures of maximum (TMD) and minimum density (TmD) are shown with red ($\triangle$) and pink (∇), respectively. The line of heat capacity maxima is shown with filled, blue circles. Melting points for specific substances are shown by violet open circle ($\circ$); C ($\lambda = 26.2$), mW ($\lambda = 23.15$), Si ($\lambda = 21$), Ge ($\lambda = 20$), Sn ($\lambda = 18.75$) and a pair-dominated SW system with $\lambda = 16$ (SW_{16}). 29

1.14 Chemical structure of some commonly used cations and anions of ionic liquids. 31

1.15 Schematic representation of excess entropy connections to the structure, thermodynamics and transport properties in complex liquids. . . 38

1.16 Schematic representation of steps involved in reverse Monte Carlo (RMC) simulations. 47

1.17 Difference in geometrical construction of the volume element for the (a) pair and (b) triplet correlation functions. r, s and t are the three inter-particle distances of a triplet and Δ is the histogram width. In the case of triplet correlation function, particle designated with 3 can move within a toroid-like volume. 54

1.18 Comparison of excess entropy obtained from thermodynamic integration using Kirkwood's coupling parameter (KCP) method with the Widom insertion method for SW liquids with varying λ at reduced temperature of 0.1926 and at zero pressure. 62

2.1 Comparison of calculated total neutron diffraction structure factor of SPC/E, TIP4P/2005 and structures generated from RMC analysis at 298 K and 0.997 g cm^{-3}. Note that structure factor of monatomic water (mW) model is not plotted here because it only represents O-O structure factor (S_{OO}) of water. 78

2.2 Normalized probability distribution of O$-$O$_c-$O angles of three water model (SPC/E, TIP4P/2005 and mW) and of RMC configurations generated at T = 298 K and ρ = 0.997 g cm^{-3}. Sharp peak at lower θ is pointed out in the figure. 79

2.3 Normalized probability distribution of tetrahedral order $P\left(q_{tet}\right)$ for all water models at (298 K, 0.997 g cm^{-3}). 80

2.4 Equilateral triplet correlation function of water oxygen atoms, $g^{(3)}_{OOO}\left(r,r,r\right)$ for all models studied, at (298 K, 0.997 g cm^{-3}). 81

2.5 The irreducible triplet correlation function, $\delta g^{(3)}_{OOO}\left(r,r,r\right) = g^{(3)}_{OOO}\left(r,r,r\right)/[g^{(2)}_{OO}\left(r\right)]^3$ for (a) molecular dynamics (MD) and (b) reverse Monte Carlo (RMC) datasets. The thin black horizontal line shows $\delta g^{(3)}_{OOO}\left(r,r,r\right) = 1$. 82

2.6 Triplet correlation functions, $g^{(3)}_{HOH}\left(r,r,r\right)$ for equilateral triangle configurations for all models studied, at (298 K, 0.997 g cm^{-3}). All correlation functions were calculated without considering any intramolecular distances of water. 83

2.7 The irreducible triplet correlation function, $\delta g^{(3)}_{HOH}\left(r,r,r\right) = g^{(3)}_{HOH}\left(r,r,r\right)/\ ([g^{(2)}_{OH}\left(r\right)]^2[g^{(2)}_{HH}\left(r\right)])$ for equilateral triangle configurations for (a) molecular dynamics (MD) and (b) reverse Monte Carlo (RMC) ensembles. The thin black horizontal line shows $\delta g^{(3)}_{HOH}\left(r,r,r\right)$ = 1. 84

2.8 Triplet correlation functions, $g^{(3)}_{OHO}(r,r,r)$ for equilateral triangle configurations for all models at (298 K, 0.997 g cm^{-3}). 84

2.9 The irreducible triplet correlation function, $\delta g^{(3)}_{OHO}(r,r,r) = g^{(3)}_{OHO}(r,r,r) \ /([g^{(2)}_{OH}(r)]^2[g^{(2)}_{OO}(r)])$ for equilateral triangles for (a) molecular dynamics (MD) and (b) reverse Monte Carlo (RMC) ensembles. The thin black horizontal line shows $\delta g^{(3)}_{OHO}(r,r,r) = 1$. . . 85

2.10 Contour plot showing isosceles triplet correlation functions, $g^{(3)}_{OOO}(r,r,t)$ as a function of the distance r and angle θ such that $t^2 = 2r^2(1-\cos\theta)$ for :(a) SPC/E, (b) TIP4P/2005 and (c) mW water models at (298 K, 0.997 g cm^{-3}). 86

2.11 Triplet correlation functions, $g^{(3)}_{OOO}(r,r,t)$ for isosceles triangle configurations for different RMC structures:(a) ASYM, (b) FREE, (c) MIX and (d) SYM. 87

3.1 Comparison of all components ($H_1(q)$, $H_2(q)$ and $H_3(q)$) of full triplet function ($\tilde{H}(q)$) calculated from molecular dynamics simulations with that of experimental results by Waseda *et al.* [223] for neon at 35.05 K temperature and 50.2 atm pressure ((a), (b) & (c)). In part (d), contribution of three components of $\tilde{H}(q)$ for liquid neon obtained from MD simulation at the same temperature and pressure is compared. 104

3.2 Full triplet functions ($\tilde{H}(q)$) obtained in our MD simulations at 35.05 K temperature and at (a) 50.2, (b) 80.7 and (c) 109.5 atm pressure with the experimental data given in Ref. 223. 105

3.3 Comparison of simulated O-O structure factor (using TIP4P/2005 and mW water model) with experimental data at 298 K temperature and at pressure P_m at (a) 500.5 bar, (b) 1510 bar, (c) 2519 bar and (d) 3319 bar. Note that in case of figure (a) and (b), the experimental pressure values are 518 bar and 1512 bar, respectively. 108

3.4 Change on peak and pre-peak intensity of O-O structure factor on application of pressure in (a) simulation using TIP4P/2005 water model and (b) experiment. 109

3.5 Comparison of simulated isothermal pressure derivative of water's O-O structure factor term ($H_3(q)$) of the triplet function, $\tilde{H}(q)$ with experimental data at 298 K and pressure P_m at (a) 500.5 bar, (b) 1510 bar, (c) 2519 bar and (d) 3319 bar. Notice that in panels (a) and (b), the experimental pressure is 518 bar and 1512 bar, respectively. 110

3.6 Effect of pressure on the isothermal pressure derivative of water's O-O structure factor, $H_3(q)$, obtained from (a) TIP4P/2005 simulations and (b) experiments. The trends with changing pressure is emphasized with the red arrows. 110

3.7 Comparison of simulated full triplet function, $\tilde{H}(q)$ with experimental data at 298 K and (a) 500.5 bar, (b) 1510 bar, (c) 2519 bar and (d) 3319 bar. Both TIP4P/2005 (red line) and the coarse-grained mW model (green line) are shown. Note that in case of (a) and (b), the experimental pressure values are 518 bar and 1512 bar respectively. . 111

3.8 Behavior of each component ($H_1(q)$, $H_2(q)$ and $H_3(q)$) of full triplet function, $\tilde{H}(q)$ in water (TIP4P/2005 water model) at 298 K temperature and (a) 500.5 bar, (b) 1510 bar (c) 2519 bar and (d) 3319 bar pressure. 113

3.9 Effect of pressure on full triplet function, $\tilde{H}(q)$, (a) in simulation using TIP4P/2005 water model and (b) in experiment at 298 K temperature. 114

3.10 Effect of pressure on O-O-O triplet correlation functions obtained from TIP4P/2005 simulations at 298 K. The TCFs associated with isosceles tri-angle configurations with probability of finding the tetrahedral angle $\approx 109.5^o$, denoted by $g^{(3)}(r, r, t)$ (where $r = s \neq t$) is plotted with solid line and the probability of finding 60^o angle, denoted by $g^{(3)}(r, r, r)$ (where $s = r = t$) is plotted with the dashed line. Note that in the first case where $r = s \neq t$, the θ is the angle formed by the two sides of same length of a triplet and is related with third length as $t^2 = 2r^2(1 - \cos\theta)$. A schematic representation of triangle configuration formed by three water molecules is specified within the plot. 115

3.11 Change in normalized probability distribution of O-O-O angles with change in pressure in simulation using TIP4P/2005 water model at 298 K. The distribution is calculated for the first coordination shell defined by a cutoff distance of 3.4 $\mathring{A}$. A schematic representation of angular arrangement of water molecules is given in the plot. 116

3.12 Normalized tetrahedral order distribution (P(q_{tet})) as function of pressure in simulation using TIP4P/2005 at 298 K. 117

4.1 Thermodynamic response functions on isobaric cooling for Stillinger-Weber (SW) and Lennard-Jones (LJ) liquids: (a) heat capacity, C_P, (b) isothermal compressibility, κ_T and (c) thermal expansion coefficient, α_P. Stillinger-Weber liquids were cooled along reduced pressure of $P = 3.2269 \times 10^{-5}$ (equivalent to 1 atm in mW unit) and Lenard-Jones liquid along $P = 1.95$. Melting temperatures in reduced units for each systems are shown with black vertical line (|) and correspond to T_m^{LJ}=0.850, $T_m^{SW_{16}}$=0.0472, T_m^{Ge}=0.0514, T_m^{Si}=0.0659 and T_m^{mW}=0.0874. Corresponding threshold temperatures are $T_{thr}^{SW_{16}}$=0.0350, T_{thr}^{Ge}=0.0300, T_{thr}^{Si}=0.0450 and T_{thr}^{mW}=0.0675. Melting temperatures are taken from the Refs. 8, 93, 96, 108, 165. For SW liquids, reduced units are taken to be in terms of well depth, ϵ and size parameter σ of the pair interaction. For the LJ system, C_P, α_P and κ_T are given in reduced units of ϵ_{LJ} and σ_{LJ}; only temperature for LJ system is reduced in terms of ϵ to ensure that all five systems fall on the same scale. 131

4.2 Excess entropy per particle, S_e as a function of temperature, T for (a) LJ (b) SW_{16}, (c) germanium (SW_{20}), (d) silicon (SW_{21}) and (e) monatomic water ($SW_{23.15}$). The excess entropy values evaluated by thermodynamic integration (TI), two-phase thermodynamic (2PT) method, and multiparticle correlation expansion (MCE) approximation are compared. The data for Lennard-Jones liquid are along P = 1.95 isobar and for Stillinger-Weber liquids are along $P = 3.2269 \times 10^{-5}$ isobar. Excess entropy obtained by Widom insertion method for SW_{16} and mW are shown with black squares (■). Melting temperature for each system is indicated with a vertical black line. For SW liquids, reduced units are taken to be in terms of well depth, ϵ and size parameter σ of the pair interaction and for LJ liquid, reduced units are taken to be in terms of ϵ_{LJ} and σ_{LJ}. 134

4.3 Heat capacity, C_P as a function of temperature for (a) LJ (b) SW_{16}, (c) germanium (SW_{20}), (d) silicon (SW_{21}) and (e) monatomic water ($SW_{23.15}$). The data for Lennard-Jones liquid are along P = 1.95 isobar and for Stillinger-Weber liquids are along $P = 3.2269 \times 10^{-5}$ isobar. Heat capacity obtained from two-phase thermodynamic method, C_P^{2PT}, pair and triplet contribution to the heat capacity, C_2 and C_3 respectively are compared. Melting temperature (T_m) and threshold temperature (T_{thr}) are shown using a vertical black line. For SW liquids, reduced units are taken to be in terms of well depth, ϵ and size parameter σ of the pair interaction and for LJ liquid, reduced units are taken to be in terms of ϵ_{LJ} and σ_{LJ}. 136

4.4 Correlation between thermodynamic excess entropy, S_e and excess entropy as a sum of pair and triplet contribution, S_{trip}, in Lennard-Jones liquid along P= 1.95 isobar and Stillinger-Weber liquids along $P = 3.2269 \times 10^{-5}$ isobar. Black dashed line is a guide to the eye for the line of slope = 1 and the points (∗) indicates the melting temperature for corresponding systems, T_m^{LJ}=0.850, $T_m^{SW_{16}}$=0.0472, T_m^{Ge}=0.0514, T_m^{Si}=0.0659 and T_m^{mW}=0.0874 taken from Refs. 8, 93, 96, 108, 165. 137

4.5 Contour plots showing isosceles triplet correlation function, $g^{(3)}(r, r, t)$ as a function of distance r and angle θi, such that $t^2 = 2r^2(1 - cos\theta)$, for Lennard-Jones liquid at pressure, P=1.95 and Stillinger-Weber liquids at $P = 3.2269 \times 10^{-5}$: (a) LJ, (b) SW_{16}, (c) germanium (SW_{20}), (d) silicon (SW_{21}) and (e) monatomic water ($SW_{23.15}$). All figures in the left column are at threshold temperature (T_{thr}) for corresponding systems, and the figures in the right column are as close to the melting temperature (T_m). 139

5.1 Loci of temperature of maximum density (TMD) and liquid spinodal (where $(\partial P/\partial V)_T = 0$, and beyond which the liquid is unstable) of monatomic water (mW), silicon (Si) and germanium (Ge) in (a) temperature−density ($T-\rho$) and in (b) pressure−temperature ($P-T$) plane. Temperature (T), pressure (P) and density (ρ) are in reduced units. 152

5.2 Thermodynamic excess entropy, S_e and pair correlation entropy, S_2 per particle as a function of density for mW ((a) & (d)), Si ((b) & (e)) and Ge ((c) & (f)) along different isotherms. The dotted black curve in each plot connects the extrema in the $S_e(\rho^*)/S_2(\rho^*)$ curves, and define the loci of excess/pair entropy anomaly in $T^* - \rho^*$ phase diagram. Note that in case of silicon and germanium, we were unable to find minima in $S_e(\rho^*)$ curves within the stable liquid region of the density range we assessed the excess entropy. 153

5.3 Tetrahedral and translational order parameters ($\langle q_{tet} \rangle$ and $\langle \tau \rangle$) for mW ((a) & (d)), Si ((b) & (e)) and Ge ((c) and (f)) along different isotherms. 154

5.4 Order map showing correlation between tetrahedral order $\langle q_{tet} \rangle$ and translational order $\langle \tau \rangle$ for (a) mW, (b) Si and (c) Ge along different isotherms. For clarity low and high density segments are indicated within the figure. 155

5.5 Behavior of transport quantities along isotherms as a function of reduced density for monatomic water ((a) diffusivity, (d) viscosity & (g) thermal conducitivity), silicon ((b) diffusivity, (e) viscosity & (h) thermal conductivity) and germanium ((c) diffusivity, (f) viscosity & (i) thermal conductivity). Note that the diffusivity and viscosity are plotted in logarithmic scale. The black dotted curve in each plot connects the extrema in the corresponding transport property vs density curve defines the locus of transport anomaly in $T^* - \rho^*$ phase diagram. The conductivity vs ρ^* plot does not show any well defined extrema within the temperature and density range we have plotted here. Note that in case of $\eta(\rho^*)$ and $\kappa(\rho^*)$ plots, the lowest accessible density is higher than in case of $D(\rho^*)$ plots because it is computed from larger simulation cells, which have higher tendency of cavitate. 156

5.6 Rosenfeld scaling of reduced self-diffusivity, D_R^* (left panels), viscosity, η_R^* (middle panels) and thermal conductivity, κ_R^* (right panels) as a function of reduced excess entropy per particle (S_e/Nk_B) for monatomic water ((a), (d) & (g)), silicon ((b), (e) & (h)) and germanium ((c), (f) & (i)). The black straight lines show the fitting of the data to Eqn. 5.3.1. The corresponding fitting equations for each branch are indicated in each plot. 159

5.7 Rosenfeld scaling of reduced self-diffusivity, D_R^* (left panels), viscosity, η_R^* (middle panels) and thermal conductivity, κ_R^* (right panels) as a function of reduced excess entropy per particle (S_e/Nk_B) for monatomic water ((a), (d) & (g)), silicon ((b), (e) & (h)) and germanium ((c), (f) & (i)) along isotherms. The black straight lines show the fitting of the data to Eqn. 5.3.1. The corresponding fitting equations for each branch are indicated in each plot. 160

5.8 Partial derivative of the thermodynamic excess entropy, as a function reduced density for (a) monatomic water (mW), (b) silicon (Si) and (c) germanium (Ge) along different isotherms. The horizontal lines in each plot corresponds to coefficient of excess entropy based conditions for finding onset of different liquid state anomalies (see Eqn. 5.3.5). The constant corresponding to the structural and density anomalies are denoted by c_s and c_ρ, respectively. For the value of c corresponding to different transport anomalies please refer to the Table 5.3. Note that wherever two branches of scaling are observed, the c value for higher density branch is considered in determining the boundary of the anomalous region. 163

5.9 Regions of anomalous behavior of the density, structural order, pair entropy, excess entropy, diffusivity, and viscosity for (a) monatomic water (mW), (b) silicon (Si) and (c) germanium (Ge) in temperature−density ($T^* - \rho^*$) plane. The symbols indicate measurements, the lines are fitted to the points and shown only as a guide to the eye. Note that the structurally anomalous region is bounded by the loci of maxima in tetrahedral order ($\langle q_{tet} \rangle$) and minima in translational order ($\langle \tau \rangle$). Notice that upper and lower boundaries of the anomalies are connected using a fitting line. Liquid spinodal line where $(\partial P/\partial V)_T = 0$ and beyond which the system is unstable is shown with red line. 165

5.10 Comparison of regions of different anomalies for monatomic water, silicon and germanium in temperature−density ($T^* - \rho^*$) plane: (a) diffusivity, (b) viscosity, (c) structural order, (d) pair entropy and (e) excess entropy. 167

5.11 Pressure−temperature ($P - T$) phase diagram of (a) mW and (b) TIP4P/2005 water models with boundaries of the density, structural, pair entropy, excess entropy and transport anomalies obtained from molecular dynamics simulation. The boundaries of the structural, density, pair entropy and diffusivity anomalies of TIP4P/2005 water model are taken from Ref. 27. The data for the phase boundaries of mW and TIP4P/2005 model are taken from Refs. 239, 266, 313, 314 respectively. The Widom line of TIP4P/2005 water model is taken from Ref. 188. Dotted lines in (a) are the metastable continuation of the corresponding coexistence line. The regions with negative and positive pressure in the phase diagram are shaded in yellow and light sky-blue, respectively. 169

5.12 Experimental pressure−temperature ($P-T$) phase diagram of germanium with boundaries of the density, structural, pair entropy, excess entropy and transport anomalies obtained from molecular dynamics simulation using SW model of germanium. The data for the phase boundaries are taken from Refs. 95,316. Liquid−liquid transition line is drawn with red line. The region with negative and positive pressure in the phase diagram is differentiated with different color. Note that temperature and pressure are in real units and conversion from mW unit to real unit was done by using energy and length scale parameter of SW-germanium: ϵ_{Ge}=45 kcal mol^{-1} and σ_{Ge}=2.186 $\mathring{A}$ [95]. 171

6.1 Chemical structures of (a) trihexyltetradecylphosphonium ($P^+_{6,6,6,14}$) cation and (b) Bromide (Br^-), (c) tetrafluoroborate (BF^-_4) and (d) dicyanamide (DCA^-) anions of the three ionic liquids used in this study. 178

6.2 Pair correlation functions (PCFs), $g(r)$, between (a) cation-cation, (b) cation-anion and (c) anion-anion for room-temperature ionic liquids ($P^+_{6,6,6,14}/DCA^-$, $P^+_{6,6,6,14}/BF^-_4$ and $P^+_{6,6,6,14}/Br^-$) at (298 K, 1 bar) and high-temperature ionic melts (NaBr, NaCl and NaF) at (1 bar, 1200 K). The PCFs of RTILs are calculated considering the phosphorous atom of the cation and central atom of the corresponding anion. . . . 183

6.3 Total and partial structure functions of (a) $P^+_{6,6,6,14}/DCA^-$, (b) $P^+_{6,6,6,14}/BF^-_4$ and (c) $P^+_{6,6,6,14}/Br^-$ ionic liquid at (1 bar, 298 K) and (d) NaBr, (e) NaCl and (f) NaF melts at (1 bar, 1200 K). 184

6.4 Spatial distribution functions (SDFs) for anion central atom (*green*, *transparent solid*) around $P^+_{6,6,6,14}$ cation in (a) $P^+_{6,6,6,14}/DCA^-$, (b) $P^+_{6,6,6,14}/BF^-_4$ and (c) $P^+_{6,6,6,14}/Br^-$ ionic liquids at 1 bar pressure and 298 K temperature. In all the cases density isovalues were chosen such that it only reflects the first solvation shell. All the SDFs are averaged over 300 frames. 186

6.5 Equilateral triplet correlation functions (ETCFs), $g^{(3)}(r,r,r)$ for cation-cation-cation ((a) & (e)), anion-anion-anion ((b) & (f)), anion-cation-anion ((c) & (g)) and cation-anion-cation ((d) & (h)) in RTILs ($P^+_{6,6,6,14}/DCA^-$, $P^+_{6,6,6,14}/BF^-_4$ and $P^+_{6,6,6,14}/Br^-$) at (1 bar, 298 K) and HTIMs (NaBr, NaCl and NaF) at (1 bar, 1200 K). 187

6.6 Potential of mean force, $V_{PMF}(r)$, as a function of cation-anion pair separation, r, for the three RTILs. The PMFs were calculated using the equation, $V_{PMF}(r) = -k_BT \ln g(r)$. Note that for calculating PMF between cation and anion in $P^+_{6,6,6,14}/DCA^-$ RTIL, the $g(r)$ between P atom of cation and center-of-mass (COM) of DCA^- anion has been used. 189

6.7 Comparison of equilateral triplet correlation functions, $g^{(3)}(r,r,r)$ (at 298 K, 1bar) for all four unique combinations calculated by dividing the full trajectory into two halves for $P^+_{6,6,6,14}/DCA^-$ ((a)-(d)) and $P^+_{6,6,6,14}/Br^-$ ((e)-(h)) RTIL. 191

6.8 Comparison of equilateral triplet correlation functions (ETCFs) for all possible unique triplets in (a) $P^+_{6,6,6,14}/DCA^-$, (b) $P^+_{6,6,6,14}/BF^-_4$, (c) $P^+_{6,6,6,14}/Br^-$ RTILs at 1 bar pressure and 298 K temperature and in (d) NaBr, (e) NaCl, (f) NaF melts at 1 bar pressure and 1200 K temperature. 192

6.9 Contour plots showing isosceles triplet correlation functions (ITCFs) for cation-cation-cation, $g^{(3)}_{cat-cat-cat}(r, r, \theta)$ (left panels) and anion-anion-anion, $g^{(3)}_{an-an-an}(r, r, \theta)$ (right panels) as a function of distance r and θ for RTILs ($P^+_{6,6,6,14}/DCA^-$ ((a) & (b)), $P^+_{6,6,6,14}/BF^-_4$ ((c) & (d)), and $P^+_{6,6,6,14}/Br^-$ ((e) & (f)) at 1 bar pressure and 298 K temperature. Note that the color scale in the contour plot for each panel is proportional to the magnitude of corresponding $g^{(3)}(r, r, \theta)$. The first and second solvation shell distances were estimated from corresponding cation-cation (for left panels) and anion-anion (for right panels) pair correlation functions and are indicated by vertical dashed line. . 193

6.10 Isosceles triplet correlation functions (ITCFs) for cation-cation-cation, $g^{(3)}_{cat-cat-cat}(r, r, \theta)$ (left panels) and anion-anion-anion, $g^{(3)}_{an-an-an}(r, r, \theta)$ (right panels) as a function of distance r and angle θ for NaBr ((a) & (d)), NaCl ((b) & (e)), and NaF ((c) & (f)) melts at 1 bar pressure and 1200 K temperature. The first and second solvation shell distances were estimated from corresponding cation-cation (for left panels) and anion-anion (for right panels) pair correlation function are indicated by vertical dashed line. 195

6.11 Isosceles triplet correlation functions (ITCFs) for anion-cation-anion, $g^{(3)}_{an-cat-an}(r,r,\theta)$ (left panels) and cation-anion-cation, $g^{(3)}_{cat-an-cat}(r,r,\theta)$ (right panels) as a function of distance r and angle θ for RTILs ($P^+_{6,6,6,14}$/DCA^- ((a) & (b)), $P^+_{6,6,6,14}$/BF^-_4 ((c) & (d)), and $P^+_{6,6,6,14}$/Br^- ((e) & (f)) at 1 bar pressure and 298 K temperature. Here the color scale in the contour plot for each panel is proportional to the magnitude of corresponding $g^{(3)}(r,r,\theta)$. The first and second solvation shell distances estimated from cation-anion pair correlation function of corresponding ionic liquids are denoted by vertical dashed line. As the structure at higher solvation shell is not so prominent, we here pictured the contour up to lower distances. 196

6.12 Isosceles triplet correlation functions (ITCFs) for anion-cation-anion, $g^{(3)}_{an-cat-an}(r,r,\theta)$ (left panels) and cation-anion-cation, $g^{(3)}_{cat-an-cat}(r,r,\theta)$ (right panels) as a function of distance r and angle θ for NaBr ((a) & (d)), NaCl ((b) & (e)), and NaF ((c) & (f)) melts at 1 bar pressure and 1200 K temperature. The first and second solvation shell distances estimated from corresponding cation-anion pair correlation function are denoted by vertical dashed line. 198

6.13 The most preferable angular orientation of anions surrounding cation head obtained from the estimation of triplet correlation functions in (a) $P^+_{6,6,6,14}$/DCA^-, (b) $P^+_{6,6,6,14}$/BF^-_4 and (c) $P^+_{6,6,6,14}$/Br^- RTILs at 298 K temperature and 1 bar pressure. Note that angular preference of anion surrounding a cation is mainly depends on the charge density on anion center and less on the size of the anion. 200

List of Tables

1.1 Melting temperature, T_m of ionic liquids with similar anions but with different cations and similar cations with different anions. 32

1.2 Potential parameters used for rigid body water models. Lennard Jones parameters of energy and length are denoted by ϵ_{OO} and σ_{OO} respectively. Intramolecular bond length and bond angle are denoted by r_{OH} and $\angle HOH$ respectively. Partial charges on oxygen and and hydrogen atoms are denoted by q_O and q_H respectively. For TIP4P/2005 water model, q_M is the charge on massless site and r_{OM} is the distance between oxygen atom and massless site. 50

1.3 BMHFT potential parameters for the three HTIMs (NaF, NaCl, NaBr) considered in this thesis. Tosi-Fumi potential parameters are taken from the Ref. 193. 53

2.1 Comparison of ensemble averaged $\langle q \rangle$ and q_{tet} values for different water models. The values of $\langle q \rangle$ have been previously reported elsewhere [81]. Numerical expressions followed for calculating both the quantities are 1.1.1 and 1.10.7 respectively. For calculation of $\langle q \rangle$ a cutoff distance 3.4 $\mathring{A}$ is used. 80

3.1 The limiting value $S(0)$ for $q \to 0$ for two water models obtained from different methods at 298 K and different pressures in molecular dynamics simulation and in experiment. The value of $S(0)$ calculated from isothermal compressibility is denoted as $S(0)^{\kappa_T}$ (see Eqn. (3.3.11)) and the values of $S(0)$ calculated from the Fourier transform method (see Eqn. (3.3.1)) and from the direct method (see Eqn. (1.10.2)) are denoted by $S(0)^{FT}$ and $S(0)^{Direct}$, respectively. In case of both the FT method and the direct method, $S(0)$ were calculated by extrapolating the corresponding structure factor from accessible q_{min} to the $q \to 0$ region. The values of $S(0)$ obtained in experiment are given by $S(0)^{Exp.}$. Note that experimental value of $S(0)^{Exp.}$ in the first two row is at 518 and 1512 bar instead of 500.5 and 1510 bar. . . 103

4.1 Key data for Stillinger-Weber and Lennard-Jones liquids. Melting temperature, T_m for SW and LJ liquids are taken from Refs. 93, 96, 108, 165 and 8. Threshold temperature below which the liquid crystalizes during a simulation run is denoted by T_{thr}. The temperatures of maximum density, T_{TMD} are taken from Ref. 96. Temperatures are shown in reduced units for all systems and in Kelvin for Ge(SW_{20}), Si(SW_{21}) and mW($SW_{23.15}$). 124

4.2 Data related to the entropy values at reference state point, T^{ref} and P^{ref} for SW and LJ liquids. In reduced units, P^{ref} = 3.2269 $\times 10^{-5}$ for SW liquids, while for LJ liquid P^{ref} = 1.95. The corresponding density at reference temperature (T^{ref}) and pressure (P^{ref}) is denoted by ρ^{ref}. The excess entropy at the reference state point is represented by S_e^{ref}. Ideal gas entropy, S_{id}^{ref} in units of k_B was calculated using ρ^{ref} following the Sackur-Tetrode formula, $S_{id}^{ref} = \frac{5}{2} - \ln\left(\rho^{ref}\Lambda^3\right)$. Excess entropy value for LJ liquid at the reference point is taken from literature [8]. Here A is the acceptance percentage for test particle insertion in Widom method. Percentage error in excess entropy calculation for SW liquids using Widom insertion method at reference state point is given in the last row. 127

4.3 Molecular dynamics simulation details for SW and LJ liquids to calculate entropy using Widom, thermodynamic integration, 2PT and MCE methods. The number of particles used for simulation is specified by N_{part}. The production run length is denoted by t_{prod}. Dumping frequency, t_{dump} refers to the frequency at which enthalpy (for TI), coordinates (for MCE), coordinates and velocity both (for 2PT) were saved during MD simulation. Thermostat and barostat relaxation time constants used for the simulation are denoted by τ_t and τ_p respectively. The superscript a is for λ=16 and 23.15, superscript b is for λ=20 and 21. 129

5.1 Computational details of molecular dynamics simulations for calculating the thermodynamics, structural quantities and diffusivity of Stillinger-Weber model of silicon, germanium and monatomic water. ρ^*_{range} and T^*_{range} are the density and temperature range studied in this work. In case of mW, at each density, the simulations are performed at temperatures every 0.00642 for the range from $T^* = 0.1155$ to $T^* = 0.1027$, and every 0.00321 for $T^* < 0.1027$. For Si, a series of simulations at different temperatures are performed at each density: starting at $T^* = 0.1252$ and decreasing T^* in intervals of 0.00642 up to $T^* = 0.1059$ and 0.00321 for $T^* < 0.1059$. For Ge, at each density the simulations are performed at temperatures every 0.00321 for the range from $T^* = 0.1059$ to $T^* = 0.0513$. Tetrahedrality parameters used for each model are denoted by λ. Equilibration and production run-lengths, denoted by t_{eq} and t_{pr} respectively are reported in units of time. 147

5.2 Molecular dynamics simulation details for calculating the viscosity and thermal conductivity of Stillinger-Weber models of silicon, germanium and monatomic water. ρ^*_{range} and T^*_{range} are the density and temperature range studied in this chapter. For mW, simulations were performed along isochores in the reduced temperature range from 0.1284 to 0.0706 in intervals of 0.00321. For Si, simulations are performed at each density, starting at $T^* = 0.1252$, and decreasing the temperature in intervals of 0.00624 up to $T^* = 0.1059$, and for $T^* < 0.1059$, with temperatures at interval of 0.00321. In case of Ge, at each density, simulations are performed at temperatures every 0.00624 for the range from $T^* = 0.1123$ to $T^* = 0.1059$ and every 0.00321 for $T^* < 0.1059$. Equilibration and production run-lengths, denoted by t_{eq} and t_{pr} respectively are reported in units of time. The lengths of the time windows over which we evaluate the PACF and HACF integrals for the calculation of viscosity and thermal conductivity, respectively, are denoted by t_η and t_κ respectively. 148

5.3 Coefficients (α) related to the Rosenfeld scaling of different transport quantities with excess entropy for monatomic water, silicon, germanium and simple liquid. The values of α for simple liquid are taken from Refs. 168, 272. Corresponding constants (c) obtained from excess entropy based criterion for observing onset of anomalies in transport quantities are also mentioned. Scaling coefficient for diffusivity, viscosity and thermal conductivity are denoted by α_D, α_η and α_κ respectively. Corresponding constants obtained from excess entropy based criterion to find onset of anomalies in diffusivity, viscosity and thermal conductivity are designated as c_D, c_η and c_κ respectively. Superscript, "a" is used for lower density branch and "b" is used for higher density branch. 164